Modelling ice characteristics in iceberg-ship collision analyses

Nicole Ferrari & Enrico Rizzuto
University of Genoa, Genoa, Italy

Alessio Prestileo
DNV GL, Høvik, Norway

ABSTRACT: The growth of commercial activities in the Arctic region, in particular of LNG transport, due to the recent discovery of new gas fields, brought to the development of new researches in the area of ice loads for ship structures. To consider possible collisions with ice during a design phase, simulations are often realized by modelling icebergs as rigid, i.e. non deformable bodies. Results obtained this way may turn out to be too conservative as the ship structure needs to be designed in order to absorb the entire amount of the impact energy. This paper describes an attempt of getting more realistic results by carrying out a collision analysis where both ice and ship are modelled as deformable. A material model describing the mechanical properties of ice is implemented in FORTRAN, for use during finite element analyses of the impact (performed using the software Abaqus CAE). The mathematical model describing ice behaviour is selected among different models present in literature. The ice model is applied in a first case to a specific situation considering a spherical iceberg of given radius impacting the side of a specific ship. The problem is decoupled, following the NORSOK method, into the analysis of a deformable iceberg impacting a rigid ship side and the analysis of the 'mirror' situation (rigid iceberg against a deformable ship). For the latter case, reference is made to results available in literature. Outputs from the two analyses are coupled, assuming that the results, separately derived, can be jointly applied to the real case of an impact between two deformable bodies. The results obtained in this first application confirm that a significant part of the impact energy is actually dissipated by ice deformation, but they are still valid under the simplifying hypothesis of neglecting the contact interactions between the two deformable bodies. The implemented material model is however ready for being integrated in the FEM analysis to study the coupled problem.

1 INTRODUCTION

Starting from the 1980s, oil and gas companies have been searching for, and finding, new gas fields in the Arctic Region: as a result, the shipping activity in this area linked to LNG has been growing. At the same time, partial ice melting made the Arctic Region easier to explore, making new sailing routes possible to be followed. However, this environment is particularly hostile due to the presence of icebergs, which can cause severe damage to the ship structures, leading to huge environmental and economic consequences. In arctic sea conditions, radars are often unable to detect icebergs being less than 2 m in height (Mejlænder-Larsen et al. 2006) therefore collisions between ships and small icebergs can easily occur. For this reason, ships sailing in the Arctic Region need to be designed to withstand ice loads.

Three different design approaches are available for assessing the damage to the structure. They are based on the definition of three cases, depending on the relative strength of the two colliding bodies and their capability of sharing the energy dissipated during the impact. These three cases are schematically represented in Figure 1.

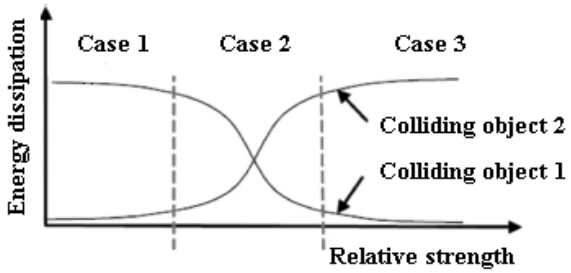

Figure 1. Energy dissipation vs relative strength.

In case 1 and 3 energy is dissipated by only one of the two colliding bodies, which is subjected to permanent deformation, whereas the second one behaves like a rigid element. In case 2, instead, both the bodies dissipate energy by permanently deforming. Case 1 and 3 are called Strength Design and Ductility Design approaches. When these concepts

are applied to iceberg-ship collisions, if a Strength Design approach is selected, ice is modelled as deformable and ship as rigid; a Ductile Design approach implies instead the opposite situation. Case 2 is called Shared-Energy Design approach and it can be followed in two ways: one way is adopting a simplified method, separately applying a Strength Design approach and a Ductile one, and then coupling the results, eventually assessing the share of deformation energy between the two objects. Results obtained this way, however, do not take into account the interactions occurring between the two bodies, which, in reality, provoke variations in the extent and geometry of the contact area during the collision. The other way is carrying out an integrated analysis where the two objects are contemporarily modelled as deformable, thus accounting for the interactions between the two bodies.

Aim of the present work was applying a Shared-Energy Design approach, adopting the NORSOK simplified method (Hoonkyu et al. 2004), to a particular iceberg-ship collision scenario. For this purpose, a deformable material model for ice was numerically implemented in FORTRAN for use in the Finite Element Software Abaqus CAE. This work is intended to be a further development of the study presented by Addario et al. (2013), who simulated a collision between a double hull LNG carrier and an iceberg by applying a Ductile Design approach (ice modelled as rigid). The purpose of the present work is, on the short term, to get an evaluation of the share of deformation energy between ice and structure following the simplified interaction approach. As it will be shown, the percentage of dissipation in ice is remarkable, and this justifies a further development of the study, with the adoption of the developed ice material model in a more complete integrated analysis.

The long term goal is to establish less conservative criteria for designing ship structures against iceberg impacts, thus obtaining more efficient and less expensive marine structures operating in ice infested waters.

2 PHYSICAL BEHAVIOUR OF ICE

Different numerical models for ice behaviour are proposed in literature, depending on the physical phenomenon to be investigated. Ice, in fact, is a very complicated material and reproducing every aspect of its behaviour using a unique mathematical model is not a realistic target. One of the models available in literature, the one proposed by Liu et al. (2011), was taken as a reference for the present work. Such model, defined empirically, is meant to represent icebergs, which are composed by freshwater ice, detached from glaciers and flown off the land into the sea. Glacier ice is the result of the compression of a great amount of snow under its own weight, until it becomes granular ice, a conglomerate of randomly oriented crystals. Thanks to this random orientation, iceberg ice can be considered as an isotropic material (Sanderson 1988).

2.1 *Parameters affecting granular ice behaviour*

Experiments showed that granular ice behaviour depends on many factors (Schulson & Duval 2009), but in the present work only some of them were considered and implemented in the material model developed in FORTRAN.

- Strain-rate: granular ice behaviour in compression has a transition from ductile to brittle at a strain rate of about 10^{-3} s^{-1}, as displayed in Figure 2 (Schulson & Duval 2009). For the adopted model (Liu et al. 2011), strain-rate dependency is only considered in an implicit way, formulating the material model as representative of high strain-rates impacts.

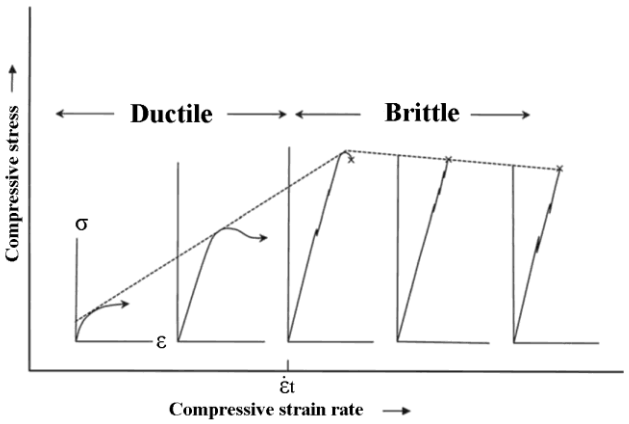

Figure 2. Schematic ice stress-strain curves at different strain-rates (Schulson & Duval 2009).

- Temperature: in case of freshwater ice, strength increases with decreasing temperature (Schulson & Duval 2009). In the present work only the case of ice at T = - 11 ºC was implemented.
- Equivalent hydrostatic pressure: it has a nonlinear influence on granular ice behaviour (Riska & Frederking 1987; Gagnon & Gammon 1995). Depending on the equivalent hydrostatic pressure, ice can stand a different amount of deviatoric stress (see § 3). Moreover, ice can resist higher compressive hydrostatic pressures than tensile ones. Influence of the equivalent hydrostatic pressure is accounted for in the definition of the material model of Liu et al. (2011)(§ 3).
- Confinement level: Kim (2014) carried out experiments on granular ice cubes studying ice behaviour depending on the confinement level. She observed that, during unconfined tests, ice failed by splitting and could no longer maintain the

load. When ice was highly confined, instead, global failure by splitting was suppressed by the boundary conditions and ice was able to stand higher loads, thus absorbing more energy. This is believed to happen because of two different ways of failing depending on the confinement level, either Coulombic or plastic (Golding et al. 2010). Coulombic faults are mainly due to shear forces at low confinement pressures, and one of the factors of the failure process is frictional sliding. Plastic faults occur instead when confinement is large enough to suppress frictional sliding and such faults are marked by plastic flow, thermal softening and solid-state re-crystallization (Schulson & Duval 2009). During a Coulombic regime, ice breaks more easily as hydrostatic pressure increases but, if the ice failure mechanism turns into plastic, ice becomes stiffer as pressure increases. During a collision with structures, ice is highly confined in the central zone of the contact area and, for this reason, it can stand high compressive pressures. Hence spall and extrusion phenomena are more likely to occur in the edge zones, where ice undergoes a Coulombic regime, rather than in the central part of the contact area (Figure 3).

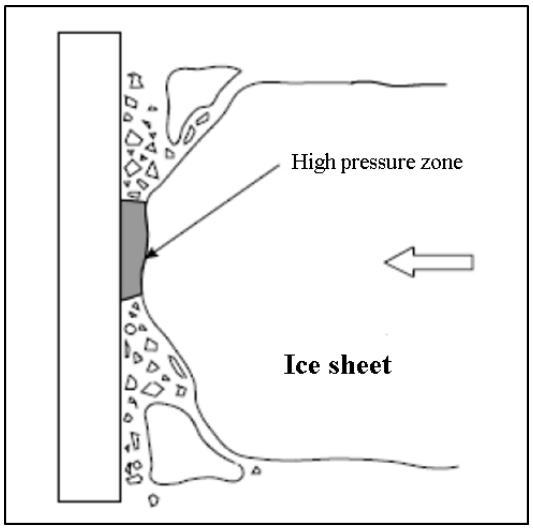

Figure 3 Schematic illustration of ice behaviour during a collision against a structure, from Jordaan (2001).

This phenomenon is taken into account in the definition of the failure criterion (§ 3.2) adopted for the selected ice material model (Liu et al. 2011).

3 NUMERICAL MODELLING OF ICE

The simplifying hypotheses described in § 2 were adopted. Moreover, for simplicity, ice behaviour was described as linear elastic-perfectly plastic and brittle in tension (Liu et al. 2011). An associated flow rule was used (see e.g. Cook et al. 2002) and plastic deformation was assumed to occur at constant volume.

The numerical model (Liu et al. 2011) is composed of a yielding function (see e.g. Cook et al. 2002) and a failure criterion.

3.1 *Yielding function*

Equation 1 is the yielding surface as proposed by Liu et al. (2011), which corresponds to the Tsai-Wu surface formulated for isotropic materials.

$$f(p,j_2) = j_2 - (a_0(T) + a_1(T)p + a_2(T)p^2) = 0 \quad (1)$$

where:

- T is temperature
- $a_0(T)$, $a_1(T)$, $a_2(T)$ are empirical parameters
- $p = -1/3\sigma_{kk}$ is the equivalent hydrostatic pressure, σ_{ij} being the generic component of the stress tensor
- $j_2 = 1/2S_{ij}:S_{ij}$, is the second invariant of the deviatoric stress tensor $\{\mathbf{S}\}$, where $S_{ij} = \sigma_{ij}-1/3\delta_{ij}\sigma_{kk}$, δ_{ij} being the Kronecker Delta

The yielding surface, for a given value of temperature, can be represented in the 3D space of the principal stresses, writing j_2 and p as:

$$p = - \sigma_{av} \quad (2)$$

$$j_2 = - [(\sigma_I - \sigma_{av})(\sigma_{II} - \sigma_{av})+(\sigma_I - \sigma_{av})(\sigma_{III} - \sigma_{av})+(\sigma_{II} - \sigma_{av})(\sigma_{III} - \sigma_{av})] \quad (3)$$

where σ_I, σ_{II} and σ_{III} are the three principal stresses and σ_{av} is the average principal stress:

$$\sigma_{av}=1/3(\sigma_I+\sigma_{II}+ \sigma_{III}) \quad (4)$$

The implicit equation of the surface, as a function of σ_I, σ_{II} and σ_{III} has the following quadratic form:

$$- [(\sigma_I - \sigma_{av})(\sigma_{II} - \sigma_{av}) + (\sigma_I - \sigma_{av})(\sigma_{III} - \sigma_{av}) + (\sigma_{II} - \sigma_{av})(\sigma_{III} - \sigma_{av})] = a_0 - a_1 \sigma_{av} + a_2 \sigma_{av}^2 \quad (5)$$

Under certain conditions (see Ferrari 2014 for details), such surface is an ellipsoid in the 3D space of the principal stresses, symmetric about the trisectrix of the first octant. The points on the trisectrix correspond to the hydrostatic condition, which occurs when all the deviatoric components of the stress tensor are zero.

The surface radius on the deviatoric plane (the plane perpendicular to the trisectrix) can be written as shown by Equation 6:

$$R(p) = \sqrt{2\left[a_2 p(d)^2 + a_1 p(d) + a_0\right]} \quad (6)$$

where d is the distance between the origin and a given point on the trisectrix.

The yielding surface selected for the present work corresponds to a temperature of -11ºC, whose parameters, derived empirically by Derradji-Aouat (2000), are listed below:

- $a_0 = 22.93$ MPa^2
- $a_1 = 2.06$ MPa
- $a_2 = -0.023$

3.1.1 *Comparison to Von Mises surface*

One of the most known yielding surfaces is the Von Mises cylinder. It is symmetrical about the trisectrix, as well as the Tsai-Wu surface (§ 3.1), but its section on the deviatoric plane does not vary; it means that the behaviour of a material represented by this surface is pressure independent. In fact, since its radius on the deviatoric plane is constant, the capability featured by the material of resisting deviatoric stress does not depend on the hydrostatic component of the stress. Moreover, the internal volume of the Von Mises surface extends with no limits following the direction of the trisectrix: as far as the stress state is hydrostatic, or close to it, the material can be indefinitely loaded.

Tsai-Wu surface does not have the same peculiarity, being instead pressure dependent. In fact, its radius on the deviatoric plane varies, until it becomes equal to zero (Equation 6). The internal volume of the Tsai-Wu surface is therefore limited, and over a certain value of the equivalent pressure stress, in tension, and below another one, in compression, the material reaches the limit even if the stress state is purely hydrostatic. Figure 4 shows the selected Tsai-Wu surface and its equivalent Von Mises cylinder (having the same maximal radius).

The radius of the Von Mises cylinder is shown in Equation 7. It only depends on the uniaxial elastic limit σ_0, which, in this case, is equal to $\sigma_0 = 14.39$ MPa (for comparison, $\sigma_0 = 235$ MPa for ordinary strength steel).

$$R_{VM} = \sqrt{\frac{2}{3}}\sigma_0 \tag{7}$$

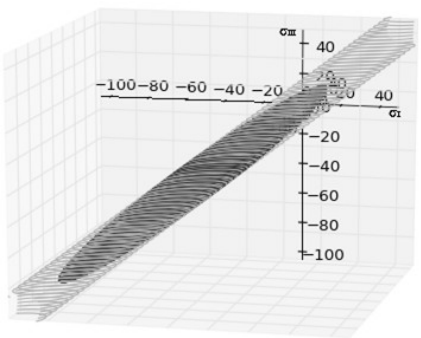

Figure 4. Selected Tsai-Wu surface and its equivalent Von Mises cylinder.

3.1.2 *Physical considerations on the yielding surface*

The one-dimensional strength corresponding to the selected yielding surface can be obtained by intersecting the surface with one of the three axes in the principal stresses space; one of the two identified intersections is ice strength in tension and the other one represents its strength in compression. Strength in tension for the considered surface ($R_t = 7.4$ MPa) is too high in comparison to experimental values (Cammaert & Muggeridge 1988). For this reason, a cut-off pressure in tension, p_{cut}, was introduced (Liu et al. 2011) in the failure criterion (see § 3.2). Without this expedient, the material model would be too conservative, since in tension ice strength would be overestimated.

The point where the chosen surface (Derradji-Aouat 2000) narrows in compression predicts the magnitude of the pressure p_{melt} causing ice to melt, and thus to instantly fail, at the considered temperature (T = - 11°C), which is about 100 MPa, as shown in Figure 5.

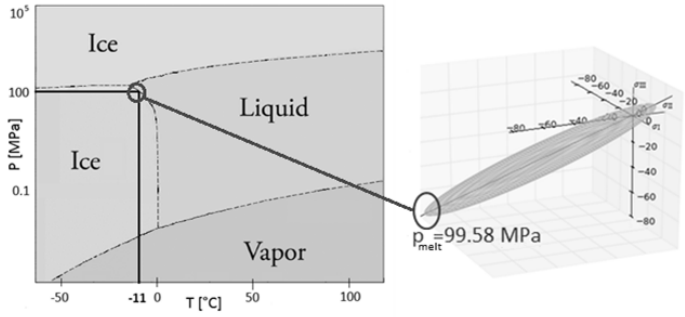

Figure 5. Correspondence between water phase diagram and selected yielding surface.

3.2 *Failure criterion*

Liu et al. (2011) proposed an empirical failure criterion, defining the amount of equivalent plastic strain that the material can withstand before failing, as a parabolic function of the equivalent hydrostatic pressure, as shown by Equation 8 and Figure 6.

$$\varepsilon_f = \varepsilon_0 + (p/p_2 - 0.5)^2 \tag{8}$$

where:

- ε_0 is the initial plastic strain, depending on experimental data, in this case equal to ε_0=0.01 (Liu et al. 2011).
- p_2 is the largest root of the yielding function in the form $f(p, j_2) = 0$ (§ 3.1) that is, in the considered case, $p_2 = 99.58$ MPa.

The amount of plastic strain to be compared to ε_f is the equivalent plastic strain, calculated as shown by Equation 9.

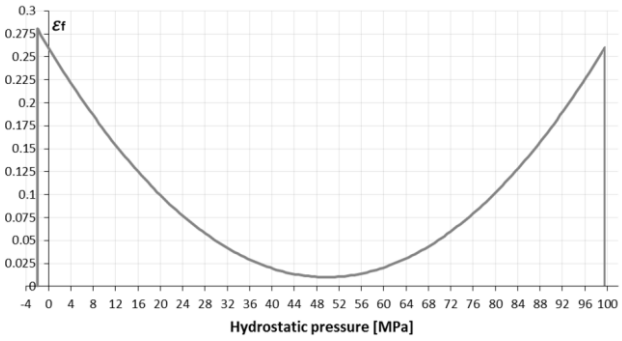

Figure 6. Pressure dependent failure criterion (Liu et al. 2011).

$$\varepsilon_{eq}^{p} = \sqrt{\frac{2}{3}\varepsilon_{ij}^{p} : \varepsilon_{ij}^{p}} \tag{9}$$

where $\{\boldsymbol{\varepsilon}^{\mathbf{p}}\}$ is the plastic strain tensor.

The cut-off pressure in tension (§ 3.1.2) is equal to p_{cut} = -2 MPa (Liu et al. 2011); it is negative because the failure criterion refers to pressure, which has opposite sign to stress (see Equation 2).

Thus, failure occurs either if $\varepsilon^{p}_{eq} > \varepsilon_f$, $p < p_{cut}$ or $p > p_{melt}$.

The U shape of the failure criterion is meant to fit experimental data, and it is consistent with the two different failure modes for ice (§ 2).

To simulate ice failure during the FEM analyses, element deletion was used in the present work: failing elements stop contributing to the stiffness of the model as if they were absent.

4 NUMERICAL IMPLEMENTATION

To carry out the present collision study, a direct explicit procedure was selected among the dynamic analyses available in Abaqus (see Ferrari 2014 and Abaqus User Manual 2014 for more details).

4.1 *Equations of motion*

The equations of motion describing the analysed system (Abaqus User Manual 2014) are generalized as shown by Equation 10.

$$[M]\{\ddot{u}\}_i^N + [C]\{\dot{u}\}_i^N + \{R^{\text{int}}\}_i = \{R^{ext}\}_i \tag{10}$$

where u^N (N = 1,…,6) is the N-th degree of freedom, [M] is the system mass matrix, [C] is its damping matrix, $\{R_{int}\}_i$ is the internal load vector, $\{R_{ext}\}_i$ is the external one and *i* indicates the time increment.

Accelerations at the beginning of the increment are computed by Abaqus solver as shown by Equation 11:

$$\{\ddot{u}\}_i^N = ([M])^{-1}(\{R^{ext}\}_i - \{R^{\text{int}}\}_i) \tag{11}$$

where $\{R_{int}\}_i$ is generated by the stress state. The explicit integration is computationally efficient due to the use of diagonal lumped mass matrices since their inverse is simple to compute.

Abaqus/Explicit uses the central-difference operator for the integration of the equations of motion (Equations 12 and 13), and the procedure is explicit in the sense that the kinematic state is determined starting from values of accelerations known from the previous increment (Equation 11).

$$\{\dot{u}\}_{i+\frac{1}{2}}^N = \{\dot{u}\}_{i-\frac{1}{2}}^N + \frac{\Delta t_{i+1} + \Delta t_i}{2}\{\ddot{u}\}_i^N \tag{12}$$

$$\{u\}_{i+1}^N = \{u\}_i^N + \Delta t_{i+1}\{\dot{u}\}_{i+\frac{1}{2}}^N \tag{13}$$

4.2 *VUMAT subroutine*

User subroutines are programming codes that can be created to increase the range of functionalities available in Abaqus. They can be written in C, C++ or FORTRAN and they are aimed at carrying out different tasks, such as the creation of new element shapes, the definition of particular kinds of contact, the description of thermal flow etc.

Abaqus/Explicit user subroutines are written with a vector interface, which means that sets of data, arranged in vectors, are exchanged between the subroutine and Abaqus solver.

In the present work, a VUMAT (vectorized user material) subroutine was chosen and written in FORTRAN. The subroutine is called by Abaqus solver at each time increment for every spatial integration point. In general, in fact, the constitutive models available in Abaqus are based on the assumption that the material behaviour is entirely defined by local effects, therefore each integration point can be treated independently (Abaqus User Manual 2014; Cook et al. 2002). When the subroutine is called, it is provided with the material mechanical condition at the beginning of the increment, which is updated by the subroutine itself.

4.3 *Ice material coding*

The inelastic response of a material can be modelled in Abaqus in two different ways, i.e. using plasticity models or adopting the damage mechanics concept. In the former case, elasticity is not affected by inelastic deformation (the Young's Module is constant during unloading and reloading beyond yielding),

while damage models include the degradation of elasticity.

The material behaviour implemented in this work is based on a plasticity model. The incremental theory was adopted during the implementation of the code, i.e. all the calculations were carried out using increments of the field variables, and not their actual values.

After a few preliminary checks (see Ferrari 2014 for details) the subroutine describing ice behaviour was implemented, according to the material model proposed by Liu et al. (2011) (§ 3): ice constitutive relation is simplified as linear elastic-perfectly plastic, the Tsai-Wu 3D surface defines the elastic limit as a function of the equivalent hydrostatic stress, and element deletion is based on a U-shaped empirical failure criterion.

The perfect plastic relation of the implemented material was treated in the present work as a particular case of the isotropic hardening behaviour applied to the Von Mises yielding surface (see e.g. Cook et al. 2002). From a 3D point of view, hardening consists of the change in the position or shape of the yielding surface in order to "follow" the point representing the stress state, which has to remain on the surface during plastic flow (while plasticity is occurring). If isotropic hardening is assumed, the surface expands of the same amount in all directions. In case of perfect plasticity, instead, no expansion occurs and the yielding function remains unchanged.

At every time increment Abaqus solver calculates the strain increment tensor using the central difference operator (Abaqus User Manual 2014), starting from the displacements (Equation 13) caused by the applied load. Starting from this datum, and from the stress tensor of the previous increment, the subroutine calculates the Von Mises equivalent stress (Equation 14) hypothesising, as a first trial, an elastic behaviour, i.e. using an elastic constitutive relation.

$$\sigma_{VM}^{trial} = \sqrt{\frac{2}{3} S_{ij} : S_{ij}} \tag{14}$$

{**S**} being the deviatoric stress tensor (§ 3.1).

If σ_{VM}^{trial} is lower than the limit, the elastic stress state is confirmed. If not, plasticity occurs and the equivalent plastic strain increment is calculated.

Since this is the case of perfect plasticity, the entire strain increment is considered as plastic: no elastic deformation occurs after yielding. The updated stress state is calculated and the total equivalent plastic strain is computed and compared to the limit imposed by the failure criterion (§ 3.2); in case such limit is exceeded, element deletion occurs.

The last step is calculating the dissipated plastic specific energy (per unit volume):

$$E_{pl}^{v} = \int_{0}^{\varepsilon_{eq}^{p}} \sigma_0(s) ds \tag{15}$$

The material constants defined for the considered material model are summarized in Table 1 (Liu et al. 2011).

Table 1. Mechanical properties of the selected ice model.

Young's module = 9500 MPa
Poisson ratio = 0.3
Density = 900 kg/m^3
Temperature = - 11°C
a_0 = 22.93 MPa^2
a_1 = 2.06 MPa
a_2 = -0.023
ε_0 = 0.01

5 ICEBERG-SHIP COLLISION ANALYSIS

As mentioned (§ 1), Addario et al. (2013) proposed a study of a collision between a double hull ship and an iceberg, for which he applied a Ductile Design approach, referring to a given impact scenario.

The present work consists of the application of a Shared-Energy approach (§ 1) to the same scenario, hence the ice material model described so far was applied to the FEM model of a deformable iceberg.

Later, the NORSOK method was applied to study the collision, taking advantage of the results about the ship energy-absorption capability derived by Addario et al. (2013).

5.1 *NORSOK method*

The NORSOK simplified method provides a way of assessing the share of deformation energy between two colliding elements and, as a consequence, to estimate the indentation they experience on each side.

Thanks to such method, load-penetration curves can be separately developed for the two bodies during two separated collision analyses: for each analysis one object is modelled as rigid, while the other one is modelled as deformable, and the deformation energy absorbed by the latter, as well as the impact force it is subjected to, are obtained as a function of the indentation it suffers.

Once the curves for the two objects are available, the only input datum necessary to assess the share of damage linked to a given collision scenario, is the total amount of deformation energy absorbed during the event, which can be obtained through the conservation of energy applied to the entire system:

$$\left(E_{kin}^{fin} + E_{abs}^{fin}\right) - E_{kin}^{init} = W_{ext} = 0 \tag{16}$$

$$E_{abs} = \Delta E_{kin} \tag{17}$$

where W_{ext} is the external work, which is zero since both the bodies involved in the impact are included in the system; E_{kin} is the total kinetic energy of the system and E_{abs} is its absorbed energy. Energy dissipations by friction between the bodies or in water, due to hydrodynamic effects, are here neglected. Results obtained adopting this assumption are conservative, since all the energy that in a real situation would be dissipated in either way, is instead modelled as entirely absorbed by the two bodies, causing larger deformations.

Given the masses of the bodies, *m* and *M,* and their initial speeds, *v* and *V*, the initial kinetic energy of the system is equal to:

$$E_{kin}^{init} = \frac{1}{2}mv^2 + \frac{1}{2}MV^2 \quad (18)$$

If the impact is supposed to be fully plastic, i.e. the two bodies do not detach after the collision, the final kinetic energy can be calculated by applying the conservation of momentum, obtaining:

$$V^* = (mv + MV)/(m + M) \quad (19)$$

$$E_{kin}^{fin} = \frac{1}{2}(m+M)(V^+)^2 \quad (20)$$

where V^* is the speed of the two attached bodies after the impact. The variation of kinetic energy ΔE_{kin} can be calculated as difference between the final and the initial one, and the total absorbed energy is equal to ΔE_{kin} (Equation 17).

The NORSOK method is based on a quasi-static assumption, according to which the forces on the two bodies during the impact are considered to be equal at every instant: $R = R_{obj1} = R_{obj2}$. Hence, the energy share between the two bodies can be assessed by calculating the sum of the areas subtended by the impact force curves, force being alike. In fact, the energy dissipated in strain within each object is equal to the area beneath each load-penetration curve: therefore the total dissipated energy E_{abs} equals the sum of the two contributions (Equation 21). When this area is identified, the indentations experienced by the two bodies can be read in the two parts of the horizontal axis. Figure 7 shows a sample application of the NORSOK method applied to an iceberg-ship collision.

$$E_{abs} = E_{abs}^{obj1} + E_{abs}^{obj2} = \int_0^{u_{obj1}^{max}} R_{obj1}\,du_{obj1} + \int_0^{u_{obj2}^{max}} R_{obj2}\,du_{obj2} \quad (21)$$

The largest limitation of the NORSOK method is that the variations in the geometry and extension of the contact area during the impact are not taken into account (interactions between the two colliding bodies are neglected). During the simulation of the iceberg deformation, in fact, ice crashes against a non deformable flat surface, which does not simulate the real behaviour of the ship side during the collision at all. The same applies for the iceberg surface, modelled as infinitely rigid when studying the deformation of the ship side: in reality, ice surface changes during the collision. This means that the method is more reliable when deformations are relatively small and, therefore, with regards to the considered scenario, when indentations are such that only the outer shell of the ship is involved in the collision.

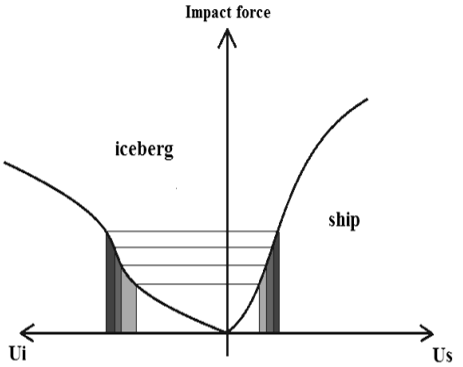

Figure 7. Sample application of the NORSOK method.

5.2 *Ship FEM model*

The ship involved in the collision study (Addario et al. 2013) is a double hull LNG carrier, with main characteristics listed in Table 2.

Table 2. Approximate ship main dimensions.

Cargo capacity ≈ 175000 m^3
Length overall ≈ 300 m
Length between perpendiculars ≈ 280 m
Breadth ≈ 45 m
Depth ≈ 25 m
Draught ≈ 12 m
Mass ≈ $1.25 \cdot 10^5$ t

Ordinary strength steel was assigned to the structure, except for the impact area, where high resistance steel was used (Addario et al. 2013).

Figure 8 shows an example of an impact analysis including a rigid sphere-shaped iceberg and the deformable ship side (Addario et al. 2013). The impact force versus indentation curve obtained in this case, neglecting friction (see § 5.1), is shown in Figure 9. Only the part of the ship curve before the outer side rupture will be considered in the following (§ 5.1).

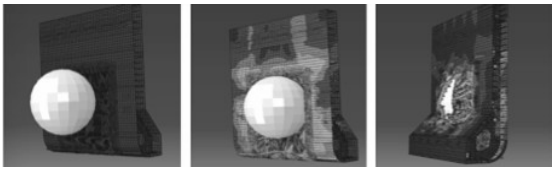

Figure 8. Impact analysis using a rigid spherical iceberg and the deformable side of the ship (Addario et al. 2013).

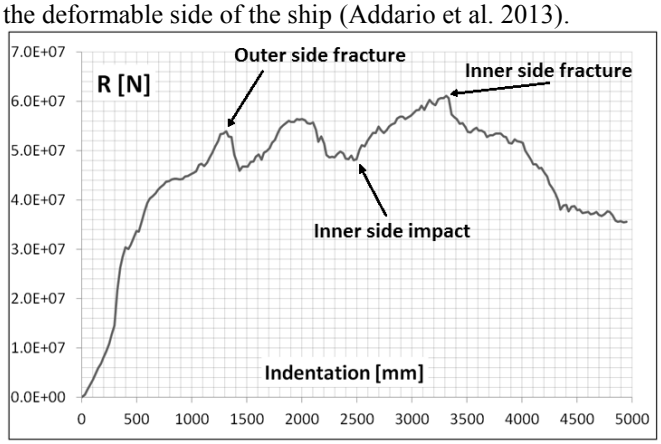

Figure 9. Impact force vs indentation curve for the ship (Addario et al. 2013).

5.3 *Analysis assumptions*

5.3.1 *Impact position and velocity components*

In case of collisions between icebergs and ships, two main scenarios can be identified: impact with a completely undetected object in the fore part of the ship, and impact during an evasive manoeuvre, in the side of the vessel (Figure 10). Moreover, ship velocity can be decomposed into two components: one in the ship longitudinal plane and the other perpendicular to it.

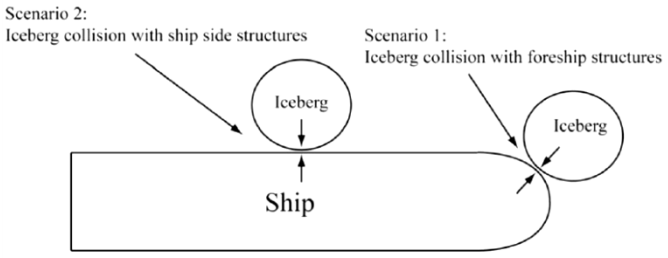

Figure 10. Possible iceberg - ship impact scenarios.

The second scenario was considered in this study and only the perpendicular component of the ship velocity was accounted for, since it is the one mostly affecting the amount of penetration into the ship side. This way, only a single degree of freedom was accounted for, i.e. the relative translation of the two objects in the transversal plane of the ship.

The vertical location of the impact was defined (Addario et al. 2013) at the ship waterline in the full load condition. Longitudinally, the impact was supposed to occur at mid-ship, between two web frames, since this scenario was expected to provide the most conservative results (Addario et al. 2013).

5.3.2 *Iceberg shape*

The iceberg overall shape is not significant, since only the portion in the impact area deforms during the collision and contributes to the energy dissipation. The local geometry in the impact area, however, may have an influence; in the present work, only a sphere-shaped iceberg was used, being the more regular surface among the ones proposed by Addario et al. (2013), therefore the more suitable for a first material testing. It was also noted that a sphere is the shape causing less localized damage to the structure, leading to smaller variations in the contact area, and to a more consistent application of the NORSOK method (§ 5.1).

5.3.3 *Velocity approach and energy balance*

Two different approaches, with regards to the impact speed during the simulation, are possible: a natural velocity and a constant velocity approach. The former is the closest to reality since it simulates the impact with a speed decreasing in time, predicting the indentation required to stop the two colliding bodies. The limit of this method is that, for every value of the variables to be investigated (initial relative speed and iceberg mass), a different analysis needs to be carried out, requiring a considerable computational effort.

A constant speed approach was chosen instead, since it can provide results, in terms of absorbed energy, which are independent on the kinetic energy, i.e. on the speed and mass of the two objects. By modelling the two objects as colliding at constant speed, a single impact force curve can be obtained for each of them, which can be used to assess the damage due to different initial conditions (using different energy values as input). The two approaches give the same results, provided the dynamic effects due to acceleration are negligible, i.e. a quasi-static condition is satisfied (Addario et al. 2013). To verify this, a quasi-static energy check (Abaqus User Manual 2014) was performed after every analysis.

The energy balance linked to the constant speed approach is shown below (Equations 22 and 23). The balance is referred to the system consisting of the deformable body, therefore the external work is, this time, different from zero, and equal to the work done to the deformable body by the rigid one.

$$(E_{kin}^{fin} + E_{abs}^{fin}) - E_{kin}^{init} = W_{ext} \tag{22}$$

$$E_{abs} = W_{ext} \tag{23}$$

Since speed is constant, and the mass loss due to damage is assumed to be negligible, the kinetic energy variation is zero. Therefore, according to Equation 23, if a collision analysis between a deformable body and a rigid one is run at constant speed, the external work done to the deformable object by the rigid one is equal to the energy absorbed by the former object.

5.4 *Deformable iceberg FEM analysis*

In order to reduce the computational effort, only a semi-sphere was modelled in Abaqus, having radius r = 5.1 m, in accordance to Addario et al. (2013). In order to generate a regular mesh in the impact area, the model was partitioned using an internal semi-sphere of radius r' = 2.5 m. The only part involved in the impact is the outer one, which was assigned linear hexahedral elements of type C3D8, having eight integration points. The mesh size in the impact area is approximately 200 mm.

The ship side was represented by a vertical wall defined as a squared analytical surface having a rigid behaviour. Its side is 10 m long and it was located at 2 mm from the impact area of the iceberg model.

The final arrangement of the collision analysis model is displayed in Figure 11.

The rear surface of the iceberg was rigidly linked to a reference point having all the degrees of freedom constrained, while the wall was forced to translate with constant speed towards the iceberg. It is preferred to impose motion to the rigid wall because it is not associated to any mass, so no kinetic energy is generated by its translation. In this way, the validity of the quasi-static assumption can simply be verified by checking the level of kinetic energy in the model, which, according to the Abaqus User Manual (2014), should be lower than 1% of the internal energy.

The wall constant speed is set to 0.5 m/s and the analysis time is chosen as equal to 3 s in order to obtain a maximal indentation of about 1.5 m.

A frictionless contact was defined between the wall and all the internal and external faces of the iceberg elements: in this way, when a layer of elements is deleted due to failure, contact between the wall and the layers beneath is granted.

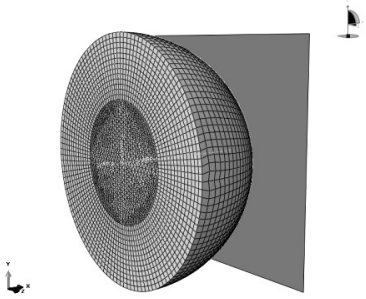

Figure 11. FEM model of deformable iceberg and rigid ship.

6 RESULTS

In this chapter the results of the collision analysis described in § 5 are shown. A sample application of the NORSOK method is then presented, in order to compare the amount of damage caused to the ship structure in the two cases of rigid and deformable iceberg, given the same total energy absorbed during the impact.

Figure 12 shows the eroded iceberg at the end of the collision analysis.

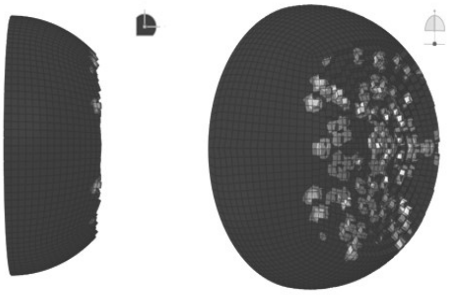

Figure 12. Eroded iceberg at the end of the impact analysis.

Results in terms of external work done on the deformable iceberg by the rigid wall, as a function of indentation, are plotted in Figure 13 (a). The impact force on ice is directly available from Abaqus as reaction force on the wall in the collision direction. Alternatively, it can be obtained by deriving the external work with respect to indentation.

In Figure 13 (b) the impact force obtained in these two ways is displayed. Its oscillating behaviour is due to the instantaneous rupture of the element layers during the impact, leading to a temporary loss of contact, which is regained as soon as the layer beneath is reached by the penetrating wall.

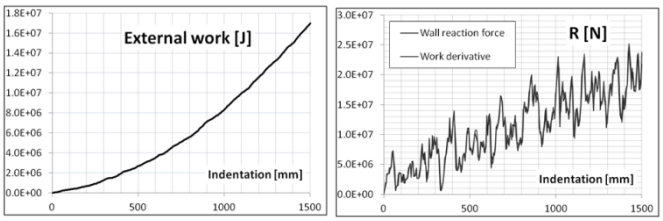

Figure 13. External work (a) and impact force (b) on deformable iceberg.

This is an intrinsic problem deriving from the discretization of the model: the finer the discretization, the less observable the oscillating phenomenon becomes. To better show this phenomenon, in Figure 14 a few frames referred to the initial instants after the impact are displayed. Contour colours refer to the contact pressure. This figure shows, in a qualitative way, the impact force variations due to the loss of contact between the two colliding bodies immediately after element deletion; grey contour indicates zero contact pressure, i.e. absence of contact.

To verify the mesh influence on the impact force oscillations, a mesh refinement of the outer layers of elements was carried out, using a mesh size of about 100 mm and running only the initial part of the collision analysis; a refinement of the entire iceberg

model and the study of a greater indentation would have caused an unnecessarily long computational time. As expected, the curve obtained using a refined mesh has more oscillations, due to the more frequent rupture of the element layers, but their amplitude is lower.

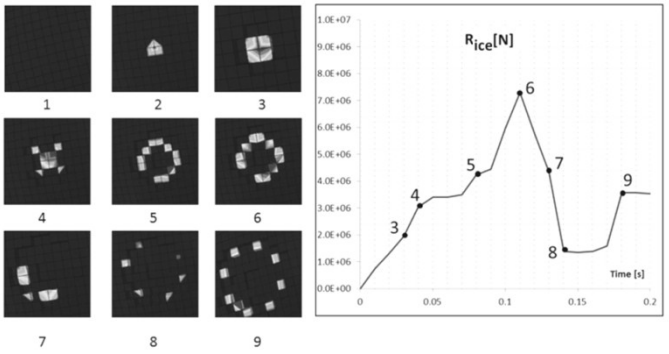

Figure 14. Contact pressure representation at the initial instants of the analysis. Frame no. 1 is the iceberg surface before impact, frame no. 2 is the impact instant.

After this verification, the curve was smoothed using a trendline based on the least squared method. A polynomial of degree 5 seemed to give the best representation of the force curve, in terms of subtended area, i.e. of absorbed energy, which is the input datum necessary to apply the NORSOK method (§ 5.1). Figure 13 shows the original curves, corresponding to the two mesh sizes, together with the interpolating function. It is here noted that the general trend of the impact force vs. indentation results to be nearly linear; this is due to the fact that the force is proportional to the sectional area of the iceberg, which, in turn, features an approximately linear increase with indentation (the latter geometrical dependence is actually quadratic, but for the dimensions under consideration the second order term has a very small effect).

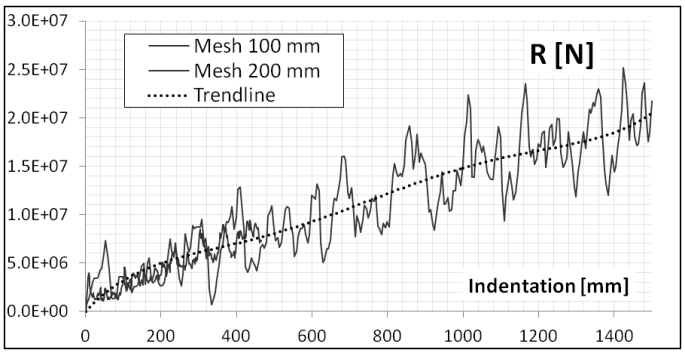

Figure 15. Impact force on ice corresponding to different mesh sizes and interpolating trendline.

6.1 *NORSOK method application*

The NORSOK method was applied, considering as input the total absorbed energy associated to a collision event causing ice to undergo a 1.5 m indentation. Such indentation corresponds to an impact force of $2.05 \cdot 10^7$ N, as visible in Figure 16. Hence, to compute the total energy absorbed during the impact (ship + iceberg), the areas subtended by the two curves, from zero force to $2.05 \cdot 10^7$ N, were calculated and summed (grey areas in Figure 13).

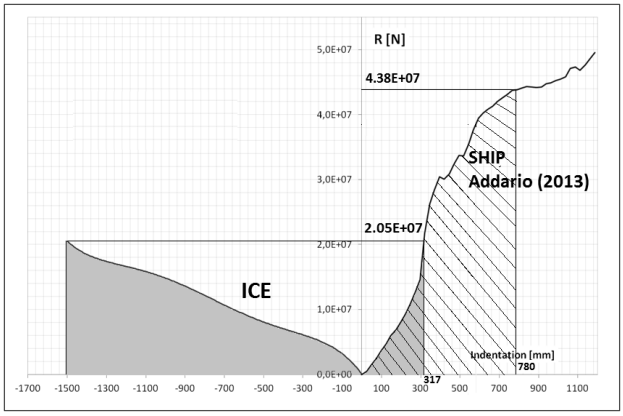

Figure 16. Impact force-indentation curves for ice and ship plotted together and their share of absorbed energy associated to the considered scenario.

The total absorbed energy is $1.93 \cdot 10^7$ J and the corresponding indentation on the ship structure is 317 mm. Ice absorbs the greater percentage of the total energy (87%). The damage to the two bodies and their energy share are summarized in Table 3.

Table 3. Energy share between iceberg and ship for the considered scenario.

	Indentation	Impact force	Absorbed energy	%
	mm	N	10^6J	
Ship	317	$2.05 \cdot 10^7$	2.44	13
Ice	1500	$2.05 \cdot 10^7$	16.8	87
Total	-	-	19.3	100

Given the total absorbed energy, it was possible to assess the damage to the ship in case a rigid iceberg is considered instead of a deformable one. This could be done by only calculating the area subtended by the ship curve until the total absorbed energy was equalled (Ductile approach: § 1). By doing so, the ship damage corresponds to 780 mm indentation, as visible in Figure 16 (hatched area).

Table 4. Shared-Energy and Ductile Design comparison.

	Shared –Energy Design			Ductile Design		
	u_i	E_{abs}	$\%E_{abs}$	u_i	E_{abs}	$\%E_{abs}$
	mm	10^6J		mm	10^6J	
Ship	317	2.44	13	780	19.3	100
Ice	1500	16.8	87	0	0	0
Total	-	19.3	100	-	19.3	100

u_i and E_{abs} are respectively indentation and absorbed energy

Table 4 shows the final results, in terms of damage to the two bodies, in the two cases of Shared-Energy Design and Ductile Design. If a deformable iceberg

is used for the considered collision analysis (Shared Energy Design), instead of a rigid one (Ductile Design), the damage caused to the ship, in terms of indentation into the structure, is about 60% lower.

6.2 *Possible impact scenarios related to the considered damage*

The absorbed energy used as input for the proposed analysis can be linked to different impact scenarios in terms of iceberg mass and ship speed. Applying the relations displayed below (Equations 24 and 25), valid for the external mechanics, and assuming the impact as fully plastic, the different combinations of these two parameters could be investigated.

$$\begin{cases} Conservation\ \ of\ \ momentum \\ Energy\ \ balance \end{cases} \tag{24}$$

$$\begin{cases} mv + MV = (m+M)V^* \\ \frac{1}{2}mv^2 + \frac{1}{2}MV^2 = \frac{1}{2}(m+M)(V^*)^2 + E_{abs} \end{cases} \tag{25}$$

Consistently with the analyses of Addario et al. (2013), the iceberg initial speed was set to v = 2 kn and V, the transversal component of the ship forward speed, was supposed to be equal to $0.1V_{ship}$. Given these two parameters and solving for the combinations of iceberg mass and initial ship speed V_{ship}, providing the same absorbed energy taken as example ($1.93 \cdot 10^7$ J: § 6.1), the curve in Figure 17 was obtained (Equations 25).

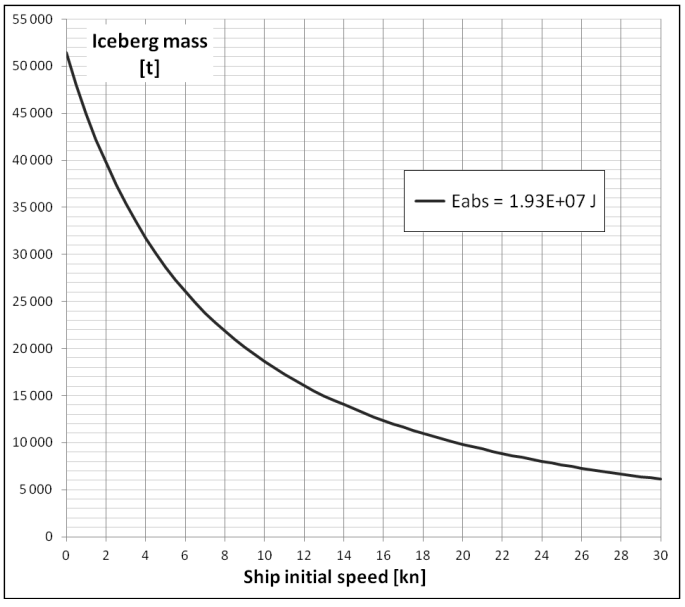

Figure 17. Combinations of iceberg mass and initial ship speed related to the studied absorbed energy amount.

7 CONCLUSIONS

A numerical model was implemented in the present study for describing ice structural behaviour during FEM simulations of collisions with floating structures.

The model was implemented using information available from literature and based on empirical data. Additional field tests should be carried out to validate the results obtained in this study. The first application of the model, however, allowed a comparison between the Shared-Energy and Ductile Design approaches, applied to a particular collision scenario between a ship and an iceberg.

The damage to the ship hull in the specific case is assessed to be about 60% less if ice deformation is modelled (ice absorbs 87% of the total energy) confirming a strong conservativeness of the Ductile Design approach, where all the energy is absorbed by the structure.

For a more precise assessment of damage, in absolute terms, frictional and hydrodynamic effects should be considered, in addition.

In the present investigation, only a spherical ice feature was studied: different iceberg shapes should be tested, in order to gain insight into the effect of this parameter and possibly choose a reference shape to be used for structural verifications.

The results presented are based on the NORSOK method, i.e. the interactions between the two bodies and the variations in the contact area and shape during the impact are ignored.

The results presented can therefore be considered as a first assessment of the influence that the application of a Shared-Energy Design approach could have on the final estimation of the ship damage during an iceberg-ship collision. Notwithstanding the simplifying assumptions, however, the results of the study clearly indicate that the energy absorption in ice is significant and cannot realistically be neglected.

To overcome the limitations of the NORSOK method, an integrated analysis should be performed, studying the simultaneous deformations of ice and structure. The model developed in the present study for describing ice structural behaviour is ready for the purpose, for use in the FEM software Abaqus/CAE, and this represent the natural development of the investigation.

REFERENCES

Abaqus User Manual 2014.

Addario, N., Rizzuto, E. & Prestileo, A. 2013. Ship Side Damage Due to Collision with Icebergs. *Developments in Maritime Transportation and Exploitation of Sea Resources*: 285-296.

Cammaert, A. B. & Muggeridge, D. B. 1988. *Ice Interaction with Offshore Structures*. New York: Van Nostrand Reinhold.

Cook, R. D., Malkus, D. S., Plesha, M. E. & Witt, R. J. 2002. *Concepts and Applications of Finite Element Analysis.* University of Wisconsin, Madison : John Wiley & Sons.

Derradji-Aouat, A. 2000. A Unified Failure Envelope for Isotropic Fresh Water Ice and Iceberg Ice. *Proceedings of the ETCE/OMAE-2000 Joint Conference, Energy for the New Millennium* OMAE2000/P&A-1002.

Ferrari, N. 2014. *Model for Ice Material Properties in Iceberg-Ship Collisions Analyses by Finite Elements.* Master's Degree Thesis. University of Genoa.

Gagnon, R. E. & Gammon, P. H. 1995. Triaxial Experiments on Iceberg and Glaciers Ice. *Journal of Glaciology* 41 (139): 528-840.

Golding, N., Schulson, E.M. & Renshaw, C.E. 2010. Shear Faulting and Localized Heating in Ice: the Influence of Confinement. *Acta Materialia* 58 (15): 5043-5056.

Hoonkyu, O., Doehyun, K., Whasoo, K., Wooil, H. & Jaehyun, K. 2004. *Safety of Membrane Type Cargo Containment System in LNG Carrier under Ice-Ship Repeated Glancing Impact of Ice.*

Jordaan, I. J. 2001. Mechanics of Ice-Structure Interaction. *Engineering Fracture Mechanics* 68 (17-18): 1923-1960.

Kim, E. 2014. *Experimental and Numerical Studies Related to the Coupled Behavior of Ice Mass and Steel Structures during Accidental Collisions.* Doctorial Thesis. NTNU.

Liu, Z., Amdahl, J. & Løset, S. 2011. Plasticity Based Material Modelling of Ice and its Application to Ship-Iceberg Impacts. *Cold Regions Science and Technology* 65(3): 326-334.

Mejlænder-Larsen, M. & Hysing, T. 2006. Dsme-DNV Jip Collision Scenario.

Riska, K. & Frederking R. 1987. Ice Load Penetration Modelling. *Proceedings of the 19th Port and Ocean Eng. under Arctic Conditions Conference:* 317-327..

Sanderson, T. J. O. 1988. *Ice Mechanics: Risks to Offshore Structures.* London: Graham and Trotman.

Schulson, E. M. & Duval, P. 2009. *Creep and Fracture of Ice.* Cambridge University Press.